Satellite Observed Sensitivity of Tropical Clouds and Moisture to Sea Surface Temperature on Various Time and Space Scales: Part 2. Focus on Marine Low Level Clouds

Erik Hojgard-Olsen, Hélène Chepfer, Hélène Brogniez

JGR Atmospheres

RESEARCH ARTICLE
10.1029/2021JD035402

Satellite Observed Sensitivity of Tropical Clouds and Moisture to Sea Surface Temperature on Various Time and Space Scales: 2. Focus on Marine Low Level Clouds

Erik Højgård-Olsen[1,2], Hélène Chepfer[1], and Hélène Brogniez[2]

[1]LMD/IPSL, Sorbonne Université, École Polytechnique, CNRS, Palaiseau, France, [2]LATMOS/IPSL, Université de Versailles Saint-Quentin-en-Yvelines, CNRS, Guyancourt, France

This article is a companion to Højgård-Olsen et al., (2022), https://doi.org/10.1029/2021JD035438

Key Points:

- Over sea surface temperature (SST) < 297 K low opaque clouds shrink vertically and horizontally with SST and the difference between low and mid-tropospheric relative humidity decreases
- Over SST > 298 K low opaque clouds lower in altitude with sea surface temperature, but keep about the same vertical extent
- Optically thin clouds are numerous in all tropical low cloud regions and rise with sea surface temperature

Supporting Information:

Supporting Information may be found in the online version of this article.

Correspondence to:

E. Højgård-Olsen,
erik.hojgard-olsen@latmos.ipsl.fr

Citation:

Højgård-Olsen, E., Chepfer, H., & Brogniez, H. (2022). Satellite observed sensitivity of tropical clouds and moisture to sea surface temperature on various time and space scales: 2. Focus on marine low level clouds. *Journal of Geophysical Research: Atmospheres*, *127*, e2021JD035402. https://doi.org/10.1029/2021JD035402

Received 14 JUN 2021
Accepted 14 FEB 2022

Abstract This study examines how satellite observed relative humidity (RH) profiles, cloud covers, and cloud altitudes vary with sea surface temperature (SST) in low cloud regions on different temporal and spatial scales over the tropical oceans (30°N–30°S). We split low clouds into optically opaque and optically thin clouds and characterize for the first time their altitude variations with SST using space lidar observations. On the process scale, the median instantaneous observations at high spatial resolution show simultaneously decreasing low opaque cloud top altitude, decreasing low opaque cloud cover, increasing middle-tropospheric RH, and decreasing lower-tropospheric RH with SST. Collectively, these observational results suggest decreasing opaque marine boundary layer cloud cover and enhanced mixing between the middle and lower troposphere with SST on the process scale, consistent with previous Large-Eddy Simulation studies. The covariations between opaque cloud cover and RH with SST are quantified on all time and space scales (from the process scale to the annual tropical mean scale). Meanwhile, on the process scale, low optically thin clouds, coexisting with opaque clouds, rise with SST (consistent with the literature mechanism), while the low optically thin cloud cover is insensitive to SST (not consistent with the literature mechanism). These results are then compared to a general circulation model, which captures the observed sign of change of opaque cloud cover and middle-tropospheric RH with SST but fails to reproduce the observed vertical shrinkage of low opaque clouds with SST and the variations of low thin clouds with SST.

Plain Language Summary Tropical low clouds, those confined to the lowest atmospheric layer, cool the planet by reflecting incoming solar radiation. Even so, it is not clear how these clouds will respond to climate changes. Previous works have run model simulations with high resolution and found that the horizontal extent of these low clouds decreases as the sea surface temperature increases, because the warmer surface causes more mixing between the lowest atmospheric layer and the layer above. We use satellite observations of high resolution and find support for both decreasing low optically thick cloud cover (horizontal extent) and more mixing as sea surface temperature increases, and we find these results on both the short and small scales, where cloud and moisture processes occur, and in annual variations over the tropical oceans. We also observe that the top of these optically thick clouds lower when sea surface temperature increases. We then compare the observed results to a climate model, which reproduces the optically thick cloud cover decrease with sea surface temperature but fails to reproduce the observed lowering of low opaque cloud tops and the overall responses of low optically thin clouds.

1. Introduction

Clouds and moisture are essential for the local and global climate, yet their responses to global warming are still not fully understood (Bony et al., 2015; Caldwell et al., 2016; Fasullo & Trenberth, 2012; Zelinka et al., 2016). Tropical low clouds cool the climate, while tropical high clouds have both cooling and warming effects. Sherwood et al. (2020) found the total uncertainty of cloud responses to global warming to be high, with comparable amounts accredited to low and high clouds. We have therefore dedicated two companion papers to separately analyze observed variations of cloud properties and relative humidity (RH) with sea surface temperature (SST) in tropical (30°N–30°S) low and high cloud situations. In the present paper (Part II), we focus on tropical low cloud situations.

The two dominating low cloud types in the tropics are (a) radiatively driven stratocumulus clouds (Sc), of typically high coverage, off the west coasts of continents, and (b) scattered cumulus clouds (Cu) in the trade-wind regions, driven by surface convection (Wyant et al., 1997).

Model-based studies (Ceppi et al., 2017; Vial et al., 2013; Zelinka et al., 2020) suggest a positive shortwave (SW) low cloud feedback from less reflection in response to decreasing cover of these clouds with warming. Estimates of this feedback are, however, associated with a large uncertainty (Bony & Dufresne, 2005; Nuijens & Siebesma, 2019; Qu et al., 2014, 2015; Vial et al., 2017), likely related to erroneous representations of Sc and Cu clouds (Klein et al., 2017; McCoy et al., 2017; Scott et al., 2020).

Observational work (Behrangi et al., 2012; Cesana, Del Genio, Ackerman, et al., 2019; Eastman et al., 2011; Höjgård-Olsen et al., 2020; Myers & Norris, 2013, 2015) place the rate of decrease of tropical marine boundary layer cloud cover with SST in a wide range (−1 to −13%/K). Recent observational analysis (Cesana & Del Genio, 2021) found high sensitivity of Sc cloud cover to SST warming (−5.1%/K), while weaker sensitivity of Cu cover (+1.4%/K).

Low cloud feedbacks are arguably sensitive to the pattern of SST warming (Fueglistaler, 2019; Loeb et al., 2020; Zhou et al., 2016, 2017), and to the temporal and spatial scale under consideration (Cesana & Del Genio, 2021; De Szoke et al., 2016): The instantaneous local view is close to the fast and small scales where cloud processes occur, while the annual global mean view is tied to global climate sensitivity. Model-based studies (Colman & Hanson, 2013; Zhou et al., 2015) have found long-term (century scale) climate feedbacks to be consistent with those derived from interannual variability. Still, that different processes and mechanisms prevail on different temporal and spatial scales (Klein & Hall, 2015; Orlanski, 1975; Steyn et al., 1981) questions the assumption of timescale-invariant and linear feedback factors (Forster et al., 2016; Mauritsen et al., 2013). Thus, Sherwood et al. (2020) raised the fundamental question of how cloud responses to variations of SST on short and local scales are tied to the long-term global climate.

On the process scale, Large-Eddy Simulation (LES) studies (Brient & Bony, 2013; Chung & Teixeira, 2012; Rieck et al., 2012; Van der Dussen et al., 2015) explain the decrease in marine boundary layer cloud cover with SST and the transitioning from Sc to Cu as follows (Kamae et al., 2016): Warmer SST leads to increased surface evaporation and latent heat flux (about +7%/K, simulated to scale with Clausius-Clapeyron), which causes more turbulent fluxes that increase the entrainment from the dry middle troposphere. Enhanced mixing with dry free-tropospheric air redistributes boundary layer moisture vertically, which deepens the boundary layer while reducing the horizontal extent of the low clouds.

In this study, we investigate the marine boundary layer mechanism from an observational perspective to understand:

1. under which specific conditions the LES-derived mechanism is valid
2. which physical mechanism dominates the observed signal on the process and annual tropical mean scales

For that purpose, we establish covariations between low clouds observed by the Cloud-Aerosol Lidar and Infrared Pathfinder Satellite Observation (CALIPSO; Winker et al., 2009), RH profiles observed by the Sounder for Atmospheric Profiling of Humidity in the Intertropics by Radiometry (SAPHIR; Brogniez et al., 2013), and SST on instantaneous and monthly timescales on the local scale, and averaged over large parts of the tropical belt on the monthly and annual scales (30°N–30°S), to answer the following questions:

1. How do tropical low cloud properties (cover and altitude) and RH profiles vary with SST on different time and space scales?
2. How are the observed physical relationships reproduced by a general circulation model in current climate and warmer climate?

Our analysis is performed under a rather novel perspective in terms of observations: We separate clouds into two different categories (opaque/thin) tied to their interaction with radiation. To keep track of the nonlinear variation, we use medians instead of simple averages to characterize the covariability of low cloud properties and RH with SST. To bridge the transition between short and local process scales and global climate, we analyze the same

data set on both the annual tropical mean scale and on the local instantaneous process scale. For the first time, we observe variations of tropical low cloud altitudes with SST using CALIPSO.

Section 2 describes the data that we use for this study and Section 3 describes how we manipulate it. We show the variables' mean states in Section 4. In Section 5, we separately analyze the responses of opaque and thin cloud covers (5.1), opaque and thin cloud altitudes (5.2), and the RH profile (5.3) to SST on various time and space scales; first from an observational perspective (a), then with model simulations (b), and finally testing the model responses to an idealized climate change forcing (+4 K warming) (c). Section 6 contains the discussion and conclusions.

2. Data

We use once daily (01:30p.m.) data of cloud properties, RH and SST collected over tropical oceans (30°N–30°S). The individual observational data sets cover different periods, highlighted below, but comparisons with results obtained over the overlapping time period (2012–2018) lead to the same conclusions. Therefore, the analyses are performed over the longest periods available for each observational data set to fully explore their records.

2.1. Observations of Clouds Properties

Cloud observations are obtained from the 1° × 1° gridded General Circulation Model-Oriented CALIPSO (Winker et al., 2009) Cloud Product V3.1.2. (Chepfer et al., 2010; Guzman et al., 2017). We separate clouds by opacity: Opaque clouds have optical depths $\tau > 3$–5 depending on the cloud microphysics and are characterized by full attenuation of the lidar beam, while thin clouds have optical depths $\tau < 3$–5 and the lidar detects a surface echo. We make use of opaque/thin cloud covers (C_{OPAQUE}, C_{THIN}) and altitudes (Z_{OpFA}, Z_{OPAQUE}, Z_{OpTOP}, and Z_{THIN}). Z_{OpFA} is the altitude where the satellite lidar beam becomes fully attenuated, Z_{OPAQUE} the emission altitude of opaque clouds, Z_{OpTOP} the altitude of opaque cloud top, and Z_{THIN} the emission altitude of thin clouds half-way between thin cloud top and base (Vaillant de Guélis et al., 2017). GOCCP data is available from April 2006, but we use data for 2008–2019 because the lidar's direction of pointing was changed slightly in November 2007, which consequently affects the homogeneity of the cloud property retrievals. Finally, we focus only on daytime measurements at 01:30p.m. local time (CALIPSO equatorial crossing time) to be consistent with Höjgård-Olsen et al. (2020) that included CloudSat observations which are only available during daytime since 2011. Moreover, we reproduced the analysis with CALIPSO nighttime data (01:30a.m.) and summarized the small differences between daytime and nighttime results in Section 6.1.

2.2. Observations of Atmospheric Relative Humidity

Observed RH is taken from the 1° × 1° gridded L2B product derived from the SAPHIR microwave radiometer onboard Megha-Tropiques (Roca et al., 2015). SAPHIR measures brightness temperatures in six channels centered around the 183.31 GHz water vapor absorption line, over a 1700 km swath with a nominal footprint resolution of 10 km at nadir (Brogniez et al., 2013; Eymard et al., 2002). RH profiles are derived from SAPHIR measurements over six atmospheric layers over 100–950 hPa (Brogniez et al., 2016; Sivira et al., 2015). Here, we make use of three layers to represent RH in the lower- (950–850 hPa), middle- (600–400 hPa) and upper (200–100 hPa) troposphere (LTRH, MTRH, UTRH, respectively). SAPHIR L2B data is available from October 2011 onward, but the instrument encountered multiple technical issues in late 2018, so we use the 2012–2018 period. Moreover, only 01:30p.m. local time observations are kept to have the same sampling as the cloud properties.

2.3. Sea Surface Temperature From Reanalysis

Sea surface temperatures (SSTs) are taken at 01:30p.m. from the average value of the 01:00p.m. and 02:00p.m. SST fields from the fifth generation of the European Centre for Medium-Range Weather Forecasts reanalysis (ERA5; Dee et al., 2011; Hoffmann et al., 2018). We consider this reanalysis product to be of appreciable accuracy, seeing as it is widely used in the community, SST is a slowly varying parameter, and previous work (Scott et al., 2020) has found variations in low cloud properties with SST to be insensitive to the use of ERA5 and NOAA SST. That said, using multiple SST reanalysis/observations can provide an additional uncertainty envelop (e.g., Cesana & Del Genio, 2021; Myers & Norris, 2016).

2.4. IPSL-CM6A General Circulation Model

In addition, we consider two sets of simulations from the IPSL-CM6A (Institut Pierre Simon Laplace – Coupled Model v6) climate model (Hourdin et al., 2006, 2020a) that runs on a 1.27° × 2.5° grid, and we analyze the 3 hourly simulations. We use simulations from the Atmospheric Model Intercomparison Project configuration ("AMIP", Ackerley et al., 2018), in which the GCM is run with prescribed time-varying SSTs and sea ice concentrations from observations. The first simulation is the AMIP run, hereafter referred to as "current climate". The second simulation is the corresponding AMIP+4K simulation (referred to as "warmer climate"), where SST has been uniformly forced to increase by +4K (Ackerley et al., 2018). Both AMIP and AMIP+4K runs are analyzed over the 2006–2014 period which overlaps the CALIPSO observational record.

These simulations include the same variables as the observational data sets (RH profiles, cloud properties, and SST). Cloud properties are simulated with the CFMIP (Cloud Feedback Model Intercomparison Project) Observation Simulator Package version 2 (COSP2; Bodas-Salcedo et al., 2011; Swales et al., 2018) lidar simulator (Chepfer et al., 2008; Guzman et al., 2017). The COSP2 lidar simulator mimics the clouds that would have been observed by the CALIPSO lidar, had it flown over the modeled atmosphere. RH in the lower, middle, and upper troposphere are extracted from the 7 standard available LMDZ outputs over 850–10 hPa and considered at 850 hPa, 500 hPa, and 150 hPa, respectively. We extract the value at 01:30p.m. each date to be consistent with the observations.

We chose to work with the IPSL-CM6A model because it has strongly improved its representation of boundary layer mixing processes during these last years (Hourdin, Rio, Jam, et al., 2020). These improvements have been evaluated against the standard CALIPSO and PARASOL cloud diagnostics originally developed in COSPV1.4 (Hourdin, Rio, Jam, et al., 2020; Madeleine et al., 2020). This model now seems to have quite an accurate representation of tropical low clouds compared to other models with respect to the cloud diagnostics originally developed in COSPV1.4 (Konsta et al., personal communication). Nevertheless, the results in Hourdin, Rio, Jam, et al. (2020) advocated for significant effort to be pursued to constrain near surface variables over tropical oceans from observations. As an attempt to contribute to this effort, we perform hereafter an evaluation of this model against observed LTRH, MTRH, UTRH as well as new cloud observational lidar diagnostics included in COSPV2 (covers and altitudes of opaque and thin clouds) that are more constraining than the original ones included in previous studies. In addition to these new diagnostics, we evaluate the model at different time and space scales to help bridge the gap between the climate scale and the process scale (supposed to be reflected in the model parameterization).

3. Method

3.1. Collocation Method

In the literature, previous studies have used satellite data collocated on different scales (annual mean, monthly mean, and instantaneously), depending on the availability of the data sets. This makes it difficult to compare results obtained from different papers. We therefore use two methods to collocate observations of cloud properties and RH; the Instantaneous Collocation Method and the Timescale Collocation Method, which allows us to assess the impact that the scale of collocation has on the results. These are described next and illustrated in Figure S1 in the Supporting Information S1.

Instantaneous Collocation Method: Orbit files of gridded cloud and RH data are collocated on the instantaneous scale. A 2-hr window around 01:30p.m. LT is applied to SAPHIR measurements when collocated with CALIPSO and ERA5 on the 1° × 1° grid box scale. The low cloud data set is extracted by keeping only grid boxes where the emission altitudes $Z_{\mathrm{OPAQUE}} \leq 3$ km and/or $Z_{\mathrm{THIN}} \leq 3$ km. This criterion precludes ascending regimes of optically thick high clouds. These instantaneous local values represent the processes at play. A temporal upscaling is performed from these instantaneously collocated observations to get monthly and annual averages. Then, spatial averages are computed from these values. These spatial averages are referred to as tropical mean values and reflect climatic-scale states. We keep a first package of 4 different tropical low cloud data sets: 2 for the local scale (instantaneous; monthly) and 2 for the tropical mean scale (monthly; annual).

Timescale Collocated Method: Monthly and annual values are computed individually for each variable for every 1° × 1° grid box and independently of the other variables. The criteria of $Z_{\mathrm{OPAQUE}} \leq 3$ km or $Z_{\mathrm{THIN}} \leq 3$ km

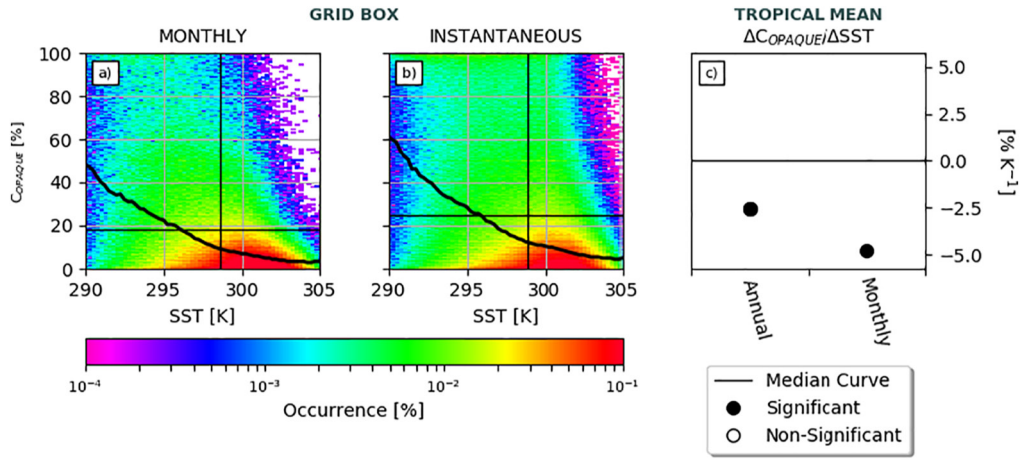

Figure 1. Density scatter plots of grid box values of opaque cloud cover vs. sea surface temperature (SST) on the local (a) monthly and (b) instantaneous timescales over the years 2008–2019 computed with the Instantaneous Collocation Method. Black curves show the median value in each SST bin. (c) Regression slopes between tropical mean C_{OPAQUE} and tropical mean SST (see also Figure S3 in the Supporting Information S1).

is then applied to the monthly and annual timescales. The spatial collocation is then performed to obtain the local and tropical mean values. Hereafter we use a second package of 2 different tropical mean low cloud data sets (monthly; annual).

Supplementary Figure S2a in the Supporting Information S1 shows the occurrence of the low cloud ($Z \leq 3$ km) data set in the all-cloud data set (i.e., all grid boxes in the instantaneously collocated data set containing any type of clouds). As expected, low clouds are observed in the subsidence regions, where they represent ∼90% of all grid boxes in the all-cloud data set. In addition, Figure S3g in the Supporting Information S1 shows that this low cloud data set only samples subsidence regimes (>20 hPa/day) and is not contaminated by deep convection. Low opaque (S2b) and low thin (S2c) clouds rarely exist alone in a 1° × 1° grid box but coexist most frequently (S2d). Low opaque clouds exist alone about equally frequently across the tropics (∼10%, S2b), apart from off the east coast of South America (35%). Meanwhile, low thin clouds exist alone in ∼20% of the cases outside of the Pacific Warm Pool.

3.2. Methods to Characterize Covariations

Figure 1 shows how low opaque cloud cover (C_{OPAQUE}) varies with SST over the 2008–2019 period, on the local (a and b) and tropical mean scales (c).

The local views (Figures 1a and 1b) show that C_{OPAQUE} decreases nonlinearly with SST on all timescales, due to the existence of different low cloud types of different sensitivities to SST over different SST ranges. To account for such nonlinearities, we use the median (black line) C_{OPAQUE} value in each SST bin to characterize the variation of low cloud properties with SST. As in Höjgård-Olsen et al. (2020), median values are computed for each 0.25 K SST bin of minimum 100 available values, and a bootstrapping algorithm (500 random samplings with replacement) removes nonsignificant values. On this local scale, median-based regressions are roughly similar across timescales (−2.5%–−4.5%/K).

Unlike the local view (1° × 1° scale), tropical means are spatially averaged values. Variations of tropical mean C_{OPAQUE} with SST are either weighted toward the most frequently observed cloud population, or toward the cloud population most sensitive to SST.

The analysis of the relationship between C_{OPAQUE} and SST on the tropical mean scale (Figure S4 in the Supporting Information S1), shows that it can be represented with a linear regression fit, whose scale factor is represented in Figure 1c. We compute the regression fits for all timescales with the publicly available orthogonal distance regression (ODR) package ODRPACK (Boggs et al., 1988, 1992; Boggs & Rogers, 1990) that accounts for measurement errors in both variables by seeking the smallest orthogonal difference between each observation

and the linear fit. We prefer to rely on ODR when we observe snapshots of the atmosphere and cannot be sure that one variable is measured without error (Leng et al., 2007; Lolli & Gasparini, 2012). Finally, the statistical significance of the linear regressions is assessed for a p value = 0.05 (Fisher, 1956).

Monthly mean local values (e.g., Figures 1a and 1b) are largely used in the literature, but studies of covariations based on this timescale mix changes in clouds and SST patterns with seasonal variability and might thus be more difficult to interpret physically than values retrieved from instantaneous and annual. Hereafter we analyze total derivatives with respect to SST. Thus, the influence of EIS is accounted for, but not shown.

The two following statements remain true for all other variables used in this study: (a) Tropical mean values vary roughly linearly with SST. (b) Similar nonlinearities are observed for the same variable on all timescales on the local scale. Henceforth in the result section (Section 5), medians (Figures 1a and 1b) are used to describe the "process scale", while scale factors from linear regression fits (Figure 1c) summarize the tropical mean rates of change.

4. Mean States

Figure 2 shows the mean states of the observed variables in the low cloud data set. It shows that as SST increases, C_{OPAQUE} (average = 45%), Z_{OpTOP} (average = 2.54 km), and Z_{OPAQUE} (average = 1.65 km) decrease. These observations suggest a transition from wide (Figure 2b) and deep (Figures 2d and 2f) low opaque clouds over cold SSTs into low opaque clouds of lower cloud tops and smaller horizontal coverage over warmer SSTs. Meanwhile, C_{THIN} is quite homogeneous (20%–40%) across the tropics. Figures 2a, 2c and 2e show the RH profiles associated to these low clouds. LTRH is high (∼80%) and MTRH is low (∼10%) where SST < 293 K. Additionally, we will use the absolute difference between LTRH and MTRH ($\mathrm{RH}_{\mathrm{DIFF}}$; Figure 2g), to discuss the mixing between the lower and middle troposphere. $\mathrm{RH}_{\mathrm{DIFF}}$ is the greatest (>65%), for SSTs < 293 K and decreases as SST increases due to both an increase in MTRH (Figure 2c) and decrease in LTRH (Figure 2e). These results are consistent with expected stronger subsidence and inversion strength over SSTs < 293 K that suppress vertical mixing and trap moisture within the boundary layer (e.g., Bretherton et al., 2013), but which weaken as SST increases.

Figure 3 represents the mean states of the same variables but for the IPSL-CM6A (AMIP) simulation. Notice that the color bar ranges differ for Figures 2 and 3. The latest version of the IPSL model (a) overestimates stratocumulus cover in the east Pacific (∼15%), (b) underestimated cloud cover in trade cumulus regimes above cloud base (∼15%), and (c) overall overestimated MTRH (7%) and underestimated UTRH (14%), while overestimated LTRH in cumulus regimes (∼10%) and underestimated LTRH in stratocumulus regimes (∼20%). These biases are consistent with analyzes in previous papers (e.g., Cesana, Del Genio, Ackerman, et al., 2019; Chepfer et al., 2008; Guzman et al., 2017; Hourdin et al., 2019; Madeleine et al., 2020).

These mean state biases may influence—but may not be the main driver of—the capability of the model to reproduce the observed clouds and RH variations with SST. In the current paper we focus on the variation with SST because they help to understand how low clouds and RH may respond to climate warming.

5. Results for Variations With SST

5.1. Cloud Covers

5.1.1. Observed Variations With SST

We first analyze how low cloud properties and RH vary with SST on different time and space scales in the observations, and then if the model reproduces the observed relationships.

Tropical mean observations (Figure 4, circles and triangles) show significant decreases in C_{OPAQUE} with SST in both collocation methods by −2.5% and −2.3%/K on the annual scale (Figure 4a), while C_{THIN} increases with SST (+0.8%/K, Figure 4b). The sensitivity of C_{OPAQUE} is larger on the monthly timescale compared to the annual (−4.5%/K vs. −2.5%/K) in both collocation methods.

Local observations (Figure 5) suggest that the tropics-wide rate of change (Figure 4, circle) reflects the decrease in C_{OPAQUE} with SST over SSTs 299–302 K on the local scales (Figure 5a), which represents the bulk of low opaque cloud observations (Figure S3a in the Supporting Information S1).

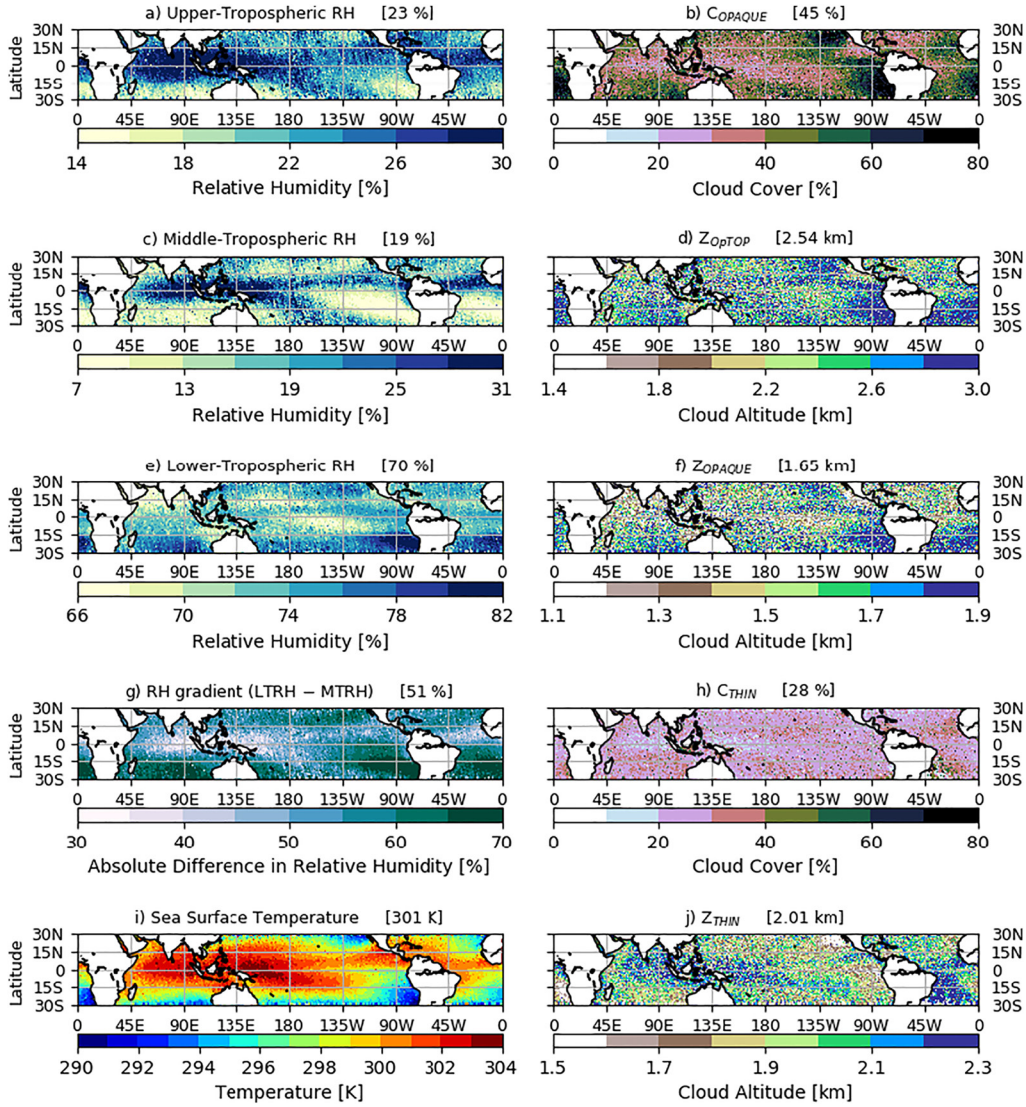

Figure 2. Observations in low cloud situations. C_{OPAQUE} (resp. C_{THIN}) is the average of C_{OPAQUE} (resp. C_{THIN}) values only in grid boxes containing opaque (resp. thin) low clouds ($C_{\mathrm{OPAQUE}} > 0\%$, $Z_{\mathrm{OPAQUE}} \leq 3$ km, resp. $C_{\mathrm{THIN}} > 0\%$, $Z_{\mathrm{THIN}} \leq 3$ km). For subplots a, c, e, and g values are averaged only over grid boxes where $Z_{\mathrm{OPAQUE}} \leq 3$ km and/or $Z_{\mathrm{THIN}} \leq 3$ km. Mean values computed with the Instantaneous Collocation Method. Tropical-wide mean values are shown in brackets in subplot titles.

The annual tropical mean scale regression for C_{OPAQUE} (−2.5%/K) that reflects the local behavior over SSTs 299–302 K, is comparable to previously published observational values; for example, −2%/K in Zhai et al. (2015), CALIPSO/CloudSat, seasonal means, 20°N/S-40°N/S), and −3.7%/K in Cesana and Del Genio (2021, CALIPSO) where −5.1%/K and +1.4%/K were attributed to Sc and Cu regions, respectively.

Indeed, the instantaneous local observations (Figure 5, top panel, blue lines) show that the median C_{OPAQUE} (5a) decreases nonlinearly with SST. Over SSTs < 293 K, the wider opaque cloud cover (∼50%, 5a) decreases rapidly with SST (−9%/K), while over SSTs > 298 K, C_{OPAQUE} is much smaller (∼10%, 5a) and decreases slowly (−1%/K for SSTs > 302 K).

The slight increase of C_{THIN} with SST (+0.8%/K, Figure 4b) on the annual tropical mean scale, likely represents the thin clouds located in the SST range 293–299 K (5b), where the local increase is +0.2%/K, and thus masks the behavior of thin clouds over SSTs > 299 K where C_{THIN} decreases by −2%/K.

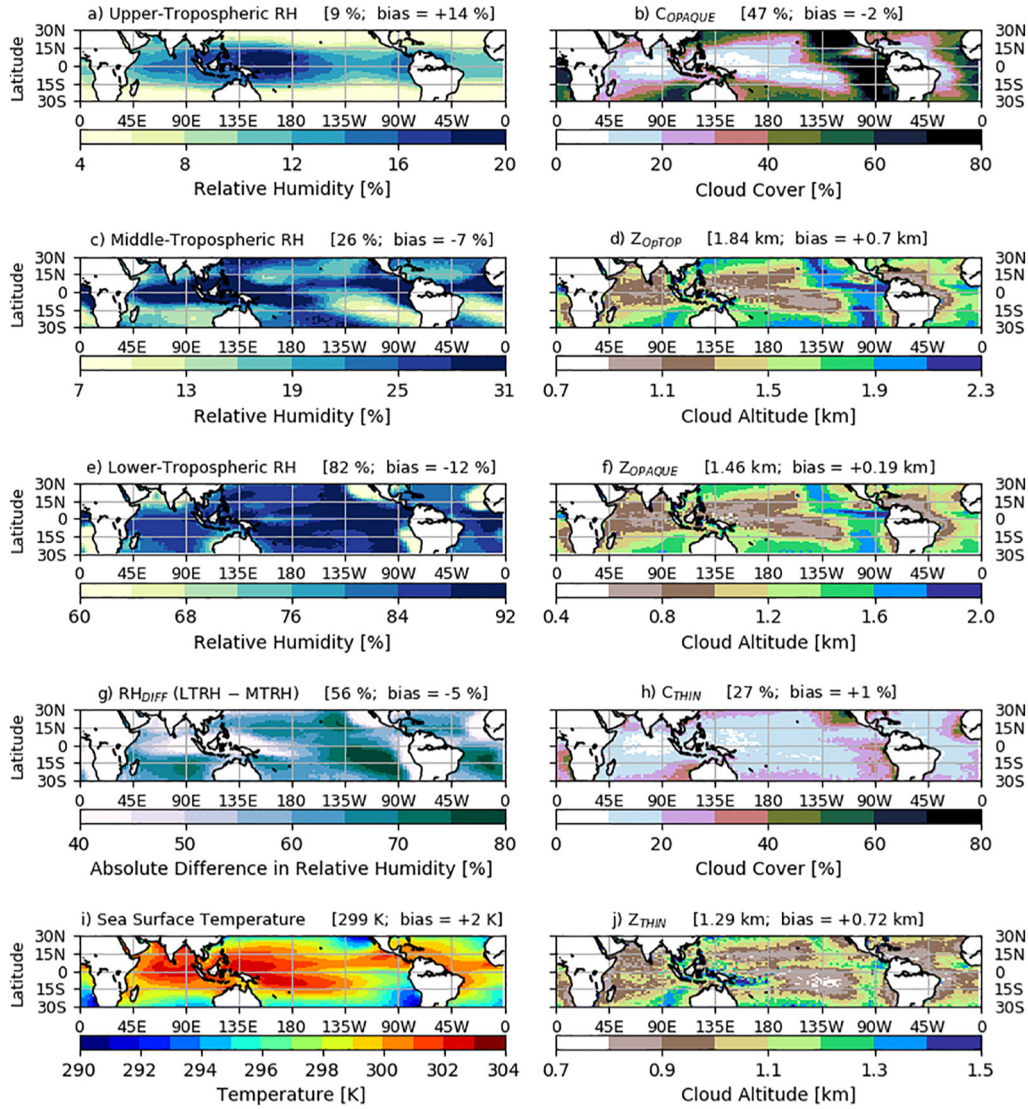

Figure 3. Same as in Figure 2, but for model current climate. Values in brackets show first the tropical-wide mean model value, and second the absolute model bias with respect to observations in tropical-wide mean. Figure S6 in the Supporting Information S1 shows the bias map.

In order to possibly identify typical behaviors of low clouds, Figure 6 is the same as Figure 5 but for specific tropical low cloud regions (shown in Figure 6e), previously defined as stratocumulus-dominated ("TrCu-Sc") and cumulus-dominated ("TrCu") regions in McCoy et al. (2017).

We checked this classification using the CASCCAD (Cumulus And Stratocumulus CloudSat-CALIPSO Data set; Cesana, Del Genio, & Chepfer, 2019) data set that separates Sc and Cu clouds. CASCCAD indicates that 3 of the 5 Sc regions in McCoy et al. (2017) are, as expected, dominated by Sc (N.E. Pacific, S.E Pacific, S.E. Atlantic), while 2 of them are dominated by Cu instead of Sc (N.E. Atlantic, S.E. Indian Ocean). We therefore moved these last two regions to the Cu category.

Figure 6 shows that we have almost no observations of TrCu clouds for SSTs < 294K, and almost no observations of TrCu-Sc for SSTs > 301 K. More interestingly, it suggests that C_{OPAQUE} decreases at the same rate in TrCu and TrCu-Sc regions over SSTs > 297 K. In contrast, over SSTs < 297 K, C_{OPAQUE} decreases with SST at a faster rate over the three most important TrCu-Sc regions ("Sc: N.E. Pacific", "Sc: S.E. Pacific", "Sc: S.E. Atlantic") than over all the TrCu regions. C_{THIN} (6c and d) is consistently insensitive to SST in all regions.

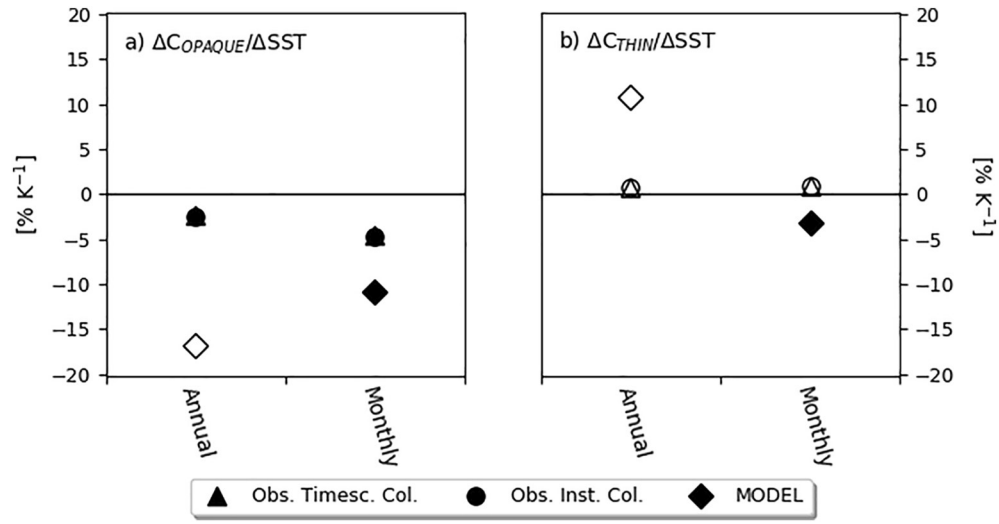

Figure 4. Slopes of linear regressions between cloud covers and SST, computed using tropical mean annual and monthly values (like Figure 2c) defined from observations (triangles and circles) and model values (lozenges). **Left**: C_{OPAQUE}. **Right**: C_{THIN}. Filled (empty) symbols represent significant (nonsignificant) values for a p value ≤ 0.05.

5.1.2. Modeled Variations With SST in Current Climate

Tropical means (Figure 4, lozenges) indicate no significant changes in modeled C_{OPAQUE} or C_{THIN} with SST on the annual mean scale, likely due to a too short annual data record. The sensitivities of monthly tropics-wide C_{OPAQUE} (−16.8%/K) and C_{THIN} (−3.2%/K) are, however, statistically significant and much larger than their observational counterparts (−4.5%/K and −0.9%/K).

The simulated low cloud cover response to surface warming is model dependent and cannot be easily generalized with other models, as previously stated in for example, Qu et al. (2014); Brient et al. (2016); Cesana, Del Genio, Ackerman, et al. (2019).

Model local instantaneous simulations (Figure 5, bottom panel, blue lines) show differences compared to the observed variations (top panel): Median C_{OPAQUE} exhibits a sharp decrease (Figure 5c) from 100% to 10% cover over a 1.5 K SST range near 298 K, which suggests a step-like function representation of the variation of C_{OPAQUE} with SST, and presumably an instant transition from stratocumulus to trade cumulus clouds in the model (discussed in Hourdin, Rio, Jam, et al., 2020), much like the LES simulations in Chung and Teixeira (2012).

Meanwhile, modeled median C_{THIN} decreases almost linearly with SST (−1.5%/K, Figure 5d) over SSTs 290–303 K, which is inconsistent with the observations where C_{THIN} is almost insensitive to SST (Figure 5b).

5.1.3. Predicted Changes in *a* +4K Warmer Climate

Figure 7 shows the difference between model simulated mean states in the AMIP+4K climate compared to the current climate (AMIP). C_{OPAQUE} (Figure 7b) decreases across the tropics (blue colors). The strongest decrease (−16%, Figure 7b) corresponds to a region, which Cesana, Del Genio and Chepfer (2019) identified as region of transition between Stratocumulus and Cu.

Overall, the −6% tropical-mean decrease in C_{OPAQUE} due to the forced +4K warming implies an average decrease of −1.5%/K. This value is much smaller than the decrease computed from the current climate simulations (Figure 4a: tropical mean monthly: −16.8%/K), and 4 times smaller than the mean change on the simulated annual local scale (−5.6%/K, Figure 5c). This suggests that in the model world, the sign of change in current climate might be an indicator of the sign of forced change in a warmer climate (Klein & Hall, 2015; Zhou et al., 2013), although the amplitude is much smaller as previously identified by Vaillant de Guélis et al. (2018) in this specific model and by Zhou et al. (2015) in other models. Qu et al. (2015, 18 CMIP5 models) simulated cloud cover responses in five low-cloud regions to increased SST over the 21st century forced by the Representative Concentration Pathway 8.5 scenario. They found that from 295.8 to 298.3 K there is an average decrease by

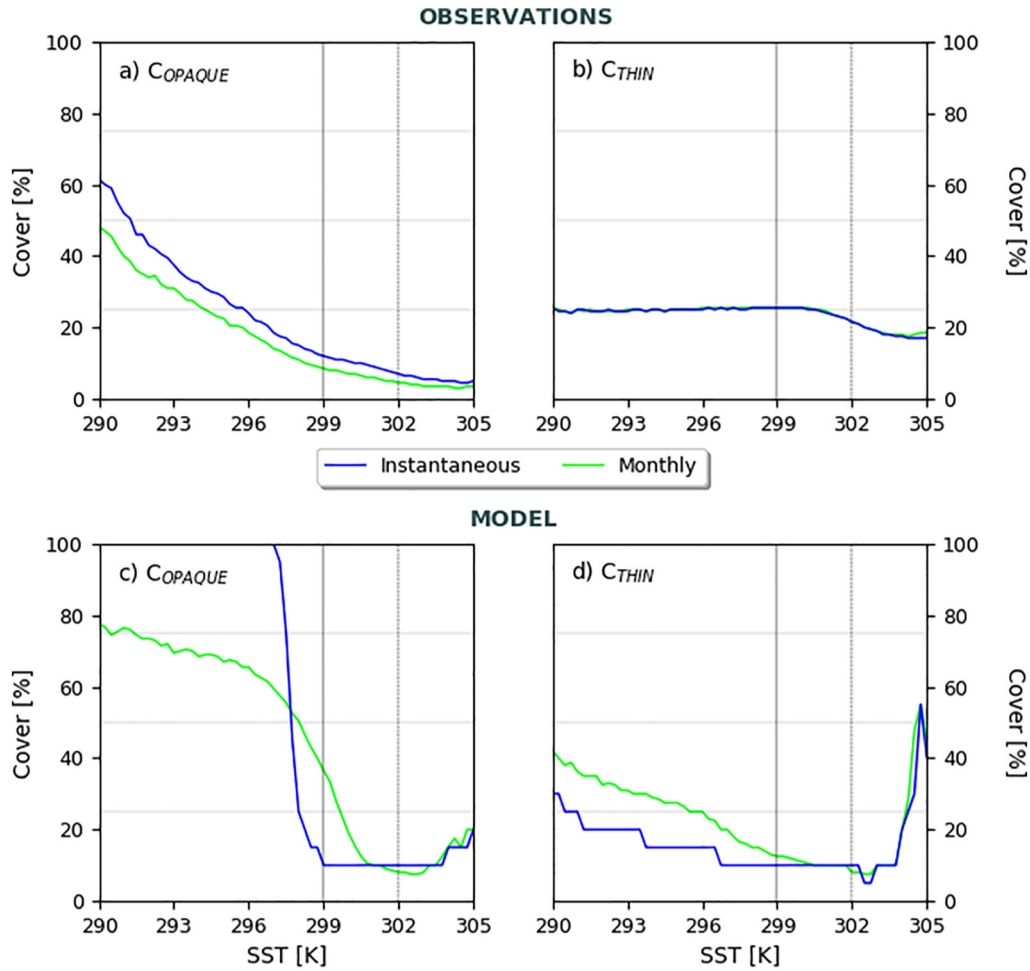

Figure 5. Variations of median C_{OPAQUE} (left column) and median C_{THIN} (right column) with sea surface temperature (SST) computed using 1° × 1° data on the instantaneous (blue) and monthly (green) timescales. The vertical dotted line at SST = 302 K marks the maximum occurrence of deep convection.

−2.9% (equivalent to −1.2%/K), which is close to the −1.5%/K response to the +4K forced warming simulated by the LMDZ model.

The forced change in C_{OPAQUE} (−6%/4K = −1.5%/K, Figure 7) seems mostly due to the Sc-to-Cu transition regions (297–299K, Figure 3) where the model current climate significantly overestimates the local rate of change (Figure 4). Assuming the model properly simulates the difference between +4K climate and current climate, then the forced change is possibly overestimated by a factor of typically 1.5, meaning −1.0%/K instead of −1.5%/K. We find that the greatest (smallest) reduction of C_{OPAQUE} in the model warmer climate in regions where we have the greatest (smallest) C_{OPAQUE} in the model current climate is consistent with the LES study by Radtke et al. (2021).

C_{THIN} forced change (−0.5%/K = −2%/4K, Figure 7h) is also due to the Sc-to-Cu transition region (297 < SST < 299K) where the observations show no sensitivity of C_{THIN} to SST (+0.2%/K, Figure 4b). Therefore, the response of C_{THIN} to forced change is possibly closer to 0 than −0.5%/K (predicted by the model).

Although we assume that if the GCM successfully replicates cloud-RH-SST relationships in the present climate, its predictions of +4 K are more trustworthy. The +4 K predictions will be affected by changes in the large-scale circulation, and the large-scale circulation change should be acknowledged as a confounding factor for analyzing the +4 K predictions (Andrews & Webb, 2018; Cesana & Del Genio, 2021; Perpina et al., 2021).

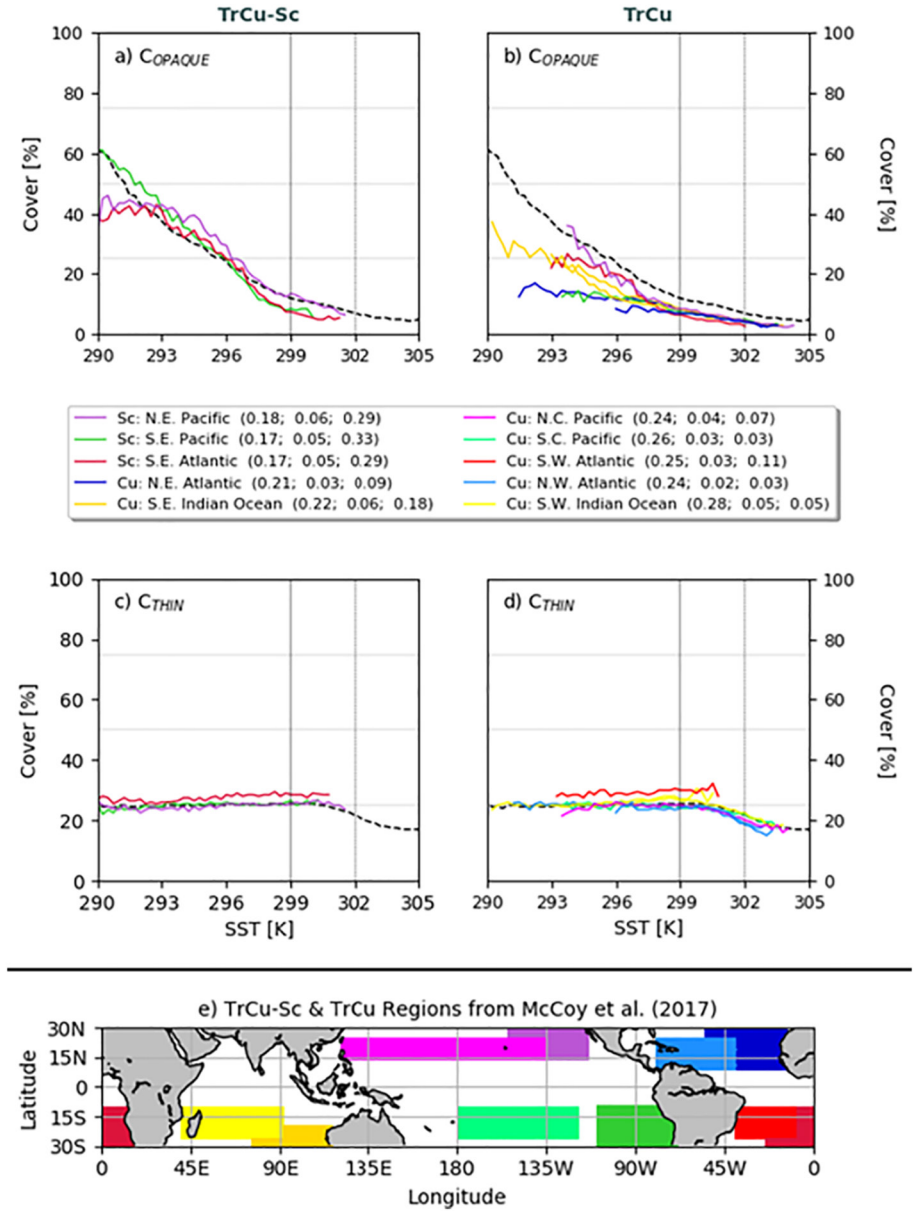

Figure 6. Regional variations of (a and b) median C_{OPAQUE} and (c and d) median C_{THIN} with sea surface temperature using 1° × 1° data on the instantaneous timescale, in regions defined in McCoy et al. (2017) as **Left**: Sc-dominated, **Right**: Cu-dominated. (e) Locations of Sc-dominated and Cu-dominated regions in McCoy et al. (2017). Numbers in parenthesis in the legend correspond to the regional multiannual mean cloud fraction values from Cumulus And Stratocumulus CloudSat-CALIPSO Data set (Cesana, Del Genio, & Chepfer, 2019), respectively for: Cumulus; Transitioning; Stratocumulus.

5.2. Cloud Altitudes

5.2.1. Observed Variations With SST

Tropical mean observations (Figure 8, circles and triangles) show significant negative monthly regressions of Z_{OPAQUE} (−25 m/K and −24 m/K) with SST increase and nonsignificant variations of Z_{THIN}, likely because the record is too short.

Local instantaneous observations (Figure 9a, top panel) show that tropical low opaque cloud altitudes decrease with SST. These results may be previously unobserved with satellite observations and indicate that tropical low opaque clouds shrink vertically as the opaque cloud top altitude decreases about −125 m/K. In contrast, thin low

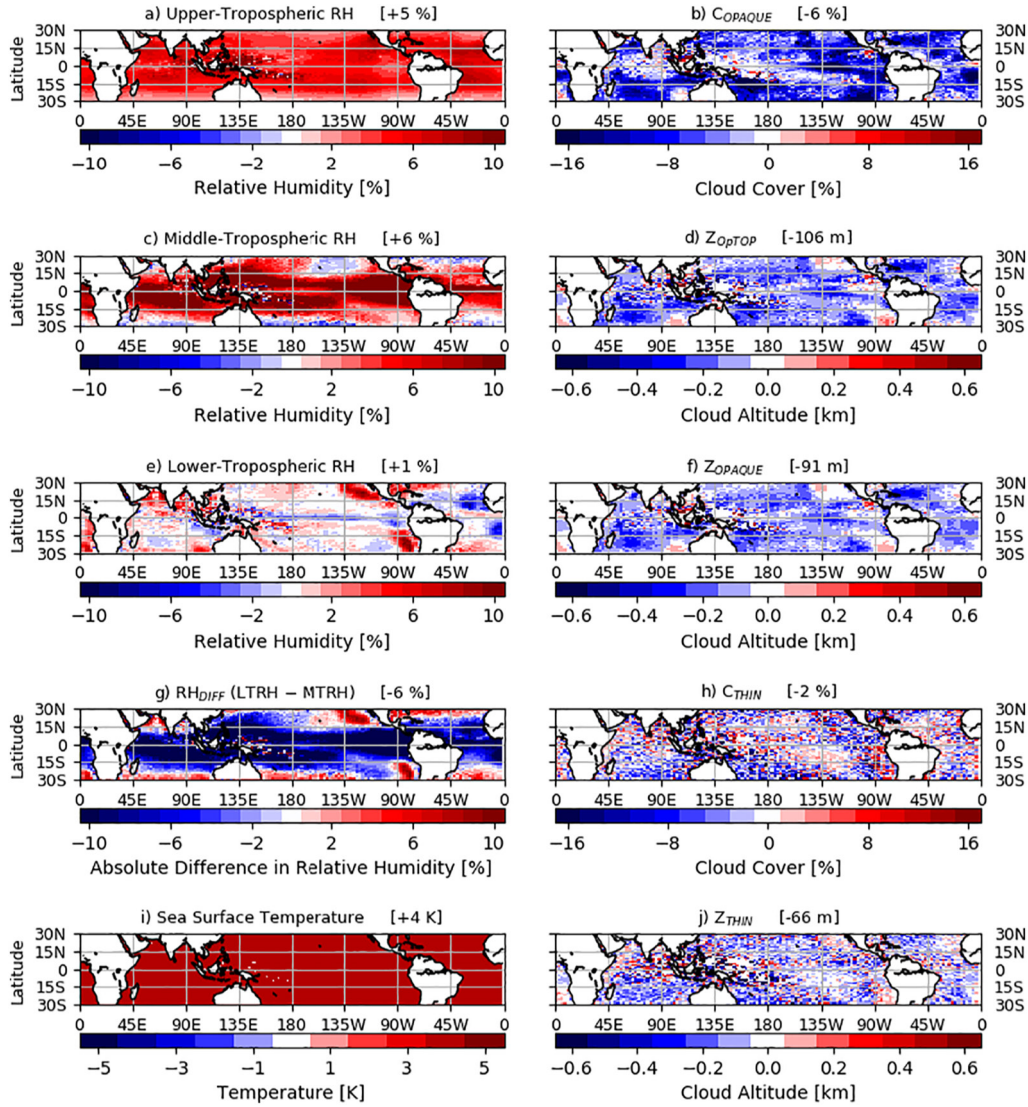

Figure 7. Absolute difference between the model warmer climate Atmospheric Model Intercomparison Project configuration (AMIP+4 K) and model current climate (AMIP) simulations. Values in brackets are the tropical-wide mean differences.

clouds rise approximately linearly with SST (+36 m/K, Figure 9b), possibly in response to both increased surface evaporation and dissipating opaque clouds.

We analyze the cloud altitudes in the regions from McCoy et al. (2017) and we found (not shown) that regional variations with SST are very similar to the all-tropics (blue curves, Figure 9) variations. However, there is a larger spread of regional Z_{OpTOP} and Z_{OPAQUE} around the all-tropics decreases (Figure 9a) in TrCu-Sc regions than in TrCu regions where they are more tightly aligned with the all-tropics decreases.

5.2.2. Modeled Variations With SST in Current Climate

Tropical means (Figure 8, lozenges) show nonsignificant annual regressions of modeled Z_{OPAQUE} and Z_{THIN} with SST, consistent with nonsignificant observed regressions. Tropical means on the monthly timescale are significant, consistent with observations of the Timescale Collocated Method (triangles).

The negative signs in simulated Z_{OPAQUE} with SST in Figure 8a are inconsistent with Zelinka et al. (2012), (2013) who found decreasing ensemble model mean cloud top pressure (−10hPa/K, about +83 m/K in a hydrostatic atmosphere) with global warming in subtropical subsidence regions.

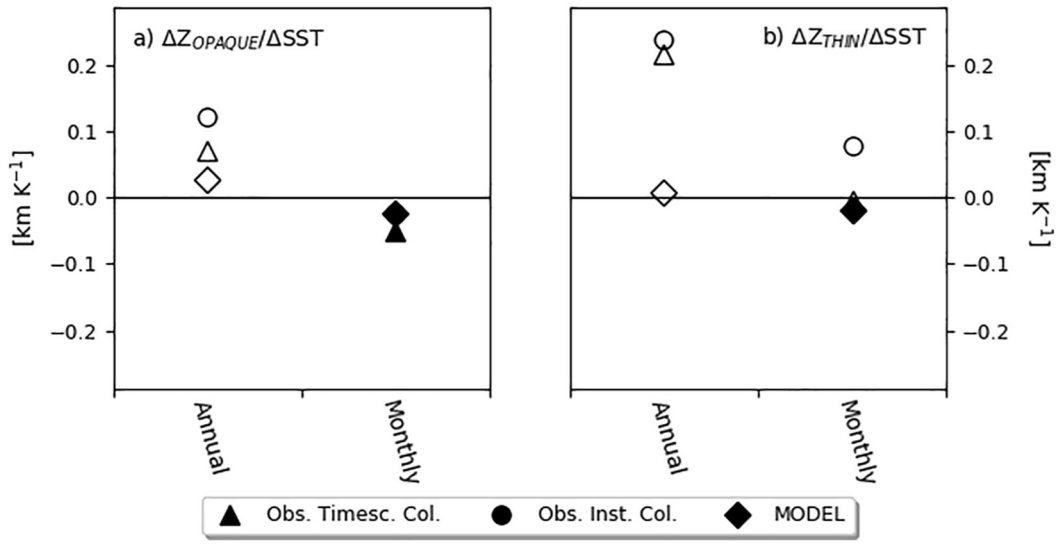

Figure 8. Same as Figure 4, but for cloud emission altitudes $\Delta Z_X/\Delta SST$. **Left:** Z_{OPAQUE}. **Right:** Z_{THIN}.

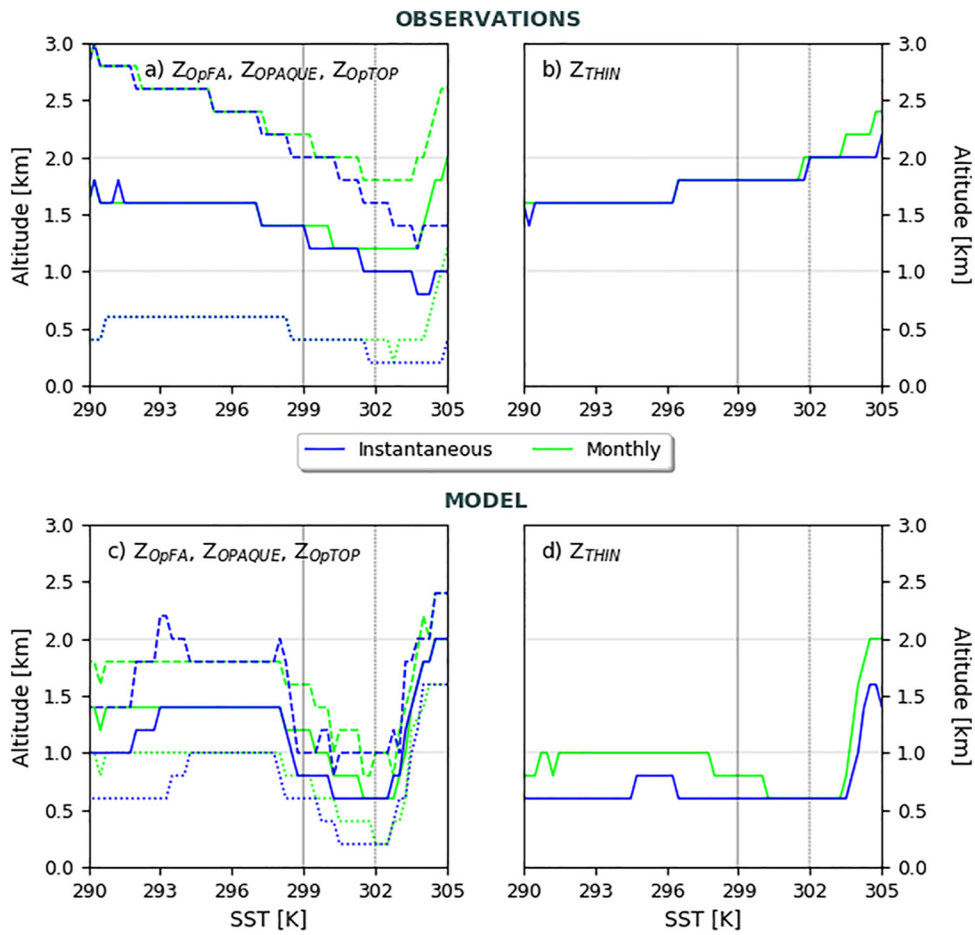

Figure 9. Same as Figure 5, but for **left** the altitude where the lidar is fully attenuated Z_{OpFA} (dotted), the altitude of opaque cloud emission Z_{OPAQUE} (solid), the altitude of opaque cloud top Z_{OpTOP} (dashed), and **right** the altitude of thin cloud emission Z_{THIN}.

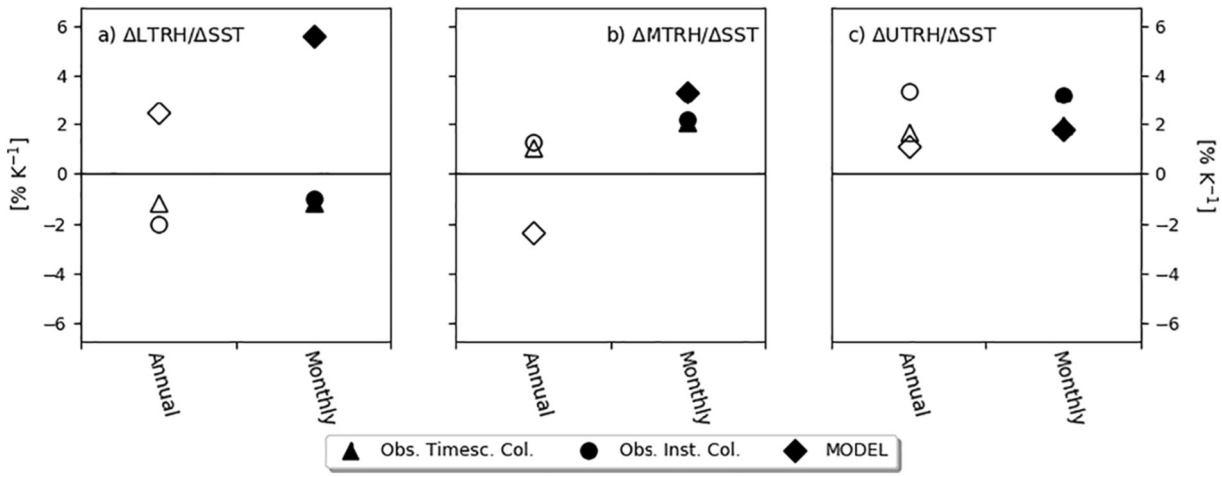

Figure 10. Same as Figure 4, but for $\Delta RH_X/\Delta SST$. (a) LTRH**,** (b) MTRH, and (c) UTRH.

Local instantaneous simulations (Figure 9c, bottom panel) show that modeled variations of Z_{OPAQUE} with SST are roughly consistent with observations over SSTs > 296 K, but not over colder SSTs. Over SSTs < 293 K, where TrCu-Sc are more numerous (Figure 6), Z_{OPAQUE} increases with SST in the model while it decreases in the observations. Modeled Z_{THIN} (Figure 9d) is basically constant, while the observed Z_{THIN} increases from 1.5 to 2.5 km over SSTs 291–305 K (Figure 9d).

5.2.3. Predicted Changes in *a* +4K Warmer Climate

The tropical-mean lowering of Z_{OPAQUE} and Z_{THIN} attributable to the +4 K warming is −23 m/K (−91 m/4K, Figure 7f) and −17 m/K (−66 m/4K, Figure 7j), respectively.

The forced change in Z_{OPAQUE} (−23 m/K, Figure 7f) seems mostly due to the Sc-to-Cu transition regions (297 < SST<299 K, Figures 3 and 7) where the model current climate simulation overestimates the local rate of change by a factor of 1.3 compared to local observations (−300 m/K instead of −225 m/K, Figure 9). Assuming the model properly simulates the difference between +4 K climate and current climate, then the forced change of Z_{OPAQUE} is possibly overestimated by a factor of 1.3 so about −18 m/K instead of −23 m/K.

Previous model-based studies using monthly global means (Zelinka et al., 2012, 2013) have reported rising low cloud altitudes with global warming. Those studies are likely relying on models whose sensitivity of Z_{OPAQUE} to SST is driven by cold SSTs (<294 K, likely Sc regions), as suggested by Cesana and Del Genio (2021), and it is thus likely too high, like the LMDz model (Figures 9a and 9c over SST < 296 K).

Because the forced change of Z_{THIN} with SST is negative (−18 m/K, Figure 7j), it can only come from the modeled Sc-to-Cu transition region where Z_{THIN} decreases with SST (297 < SST < 299 K, Figure 9d). However, this decreasing Z_{THIN} does not exist in reality, as shown in the observations (Figure 9b). Therefore, the tropical mean model prediction of Z_{THIN} is likely not reliable.

5.3. RH With SST

5.3.1. Observed Variations With SST

Tropical means (Figure 10, circles and triangles) show that monthly tropical mean LTRH decreases with SST (−1.2%/K, Figure 10a), while monthly MTRH and UTRH increase (+2.2 Figure 10b, and +3.2%/K, Figure 10c). Previous observational works have concluded that there are no significant trends in large-scale UTRH over ocean surfaces in clear-sky situations (Bates & Jackson, 2001; Shi & Bates, 2011), but Figure 10 shows significant slopes of regressions of monthly RH at all levels in tropical low cloud situations.

Local instantaneous observations (Figure 11, top panel) show linearly decreasing LTRH (−1.3%/K, Figure 11a), while increasing UTRH (+1.1%/K, Figure 11c) over SSTs 290–302 K. Simultaneously, MTRH increases

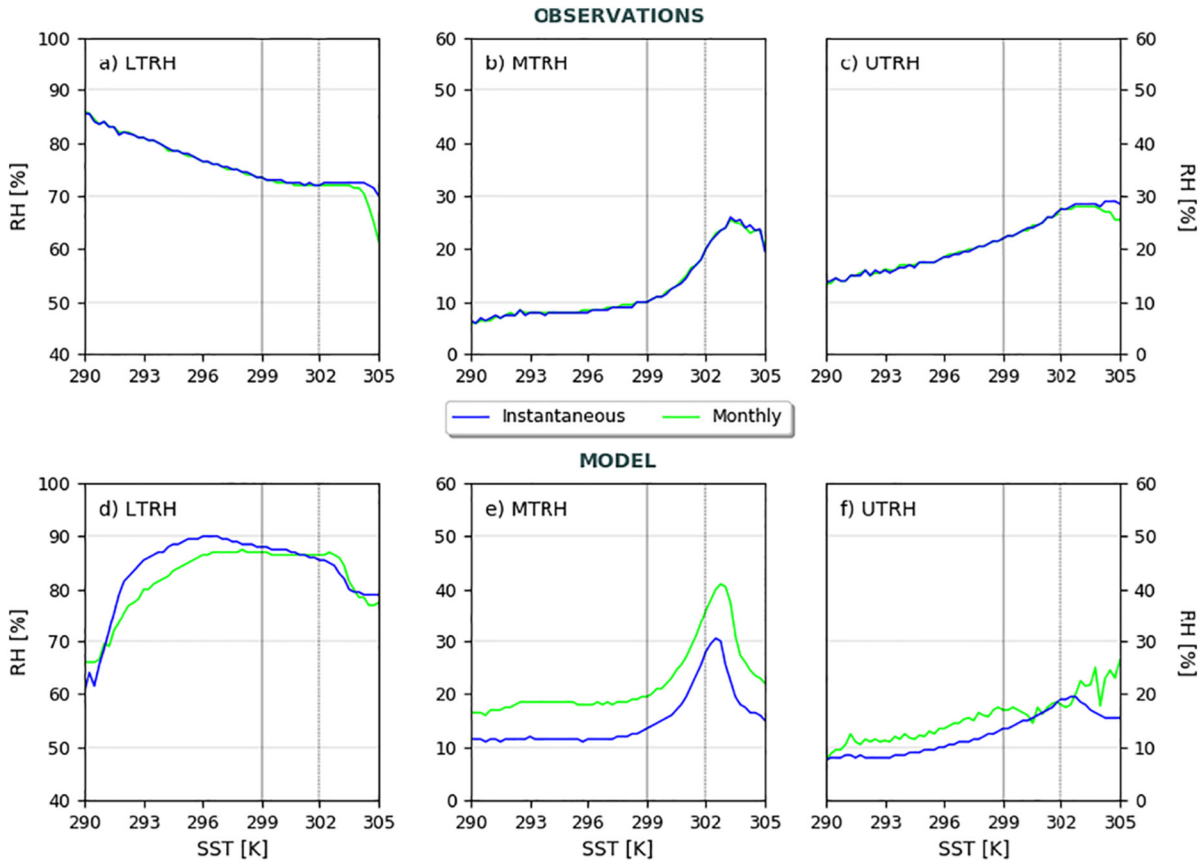

Figure 11. Same as Figure 5, but for **Left** LTRH, **Middle** MTRH, and **Right** UTRH.

nonlinearly with SST (Figure 11b) with a significant pick-up around 299 K. The variations of LTRH and MTRH yield a linear decrease in RH_{DIFF} over SSTs between 290 and 301 K (Figure S5 in the Supporting Information S1).

5.3.2. Modeled Variation With SST in Current Climate

Tropical means (Figure 10, lozenges) show that the model simulates significant positive regressions on the monthly timescale (LTRH = +5.6%/K; MTRH = +3.3%/K; UTRH = +1.8%/K), which is consistent with increasing MTRH and UTRH in the observations, but inconsistent with decreasing LTRH.

The positive simulated regressions of the RH profile in Figure 10 are consistent with Sherwood et al. (2010; 18 coupled ocean-atmosphere CMIP3 models) who simulated positive tropical (30°N–30°S) ensemble-mean increases. In Figure 10 we simulate positive regressions with only the IPSL model in tropical low cloud regions.

Local instantaneous simulations (Figure 11, bottom panel) show tendencies that resemble the observational variations (top panel) of MTRH and UTRH, although magnitudes and locations of peak notations differ. Most notable are the local variations in simulated LTRH (Figure 11d): In contrast to linearly decreasing LTRH in the observations (Figure 11a), modeled LTRH (Figure 11d) initially increases sharply (+13%/K) until SST ≈ 296K, and then decreases slightly over SSTs > 296 K. The variations of LTRH and MTRH with SST yield an increase in RH_{DIFF} for SSTs between 290 and 297 K and a decrease for SSTs > 297 K.

The inconsistency between observed and modeled LTRH (Figures 10a and 11d) might be physical, or due to the thickness differences in the LTRH layers in observations (850–950 hPa) and model (850 hPa) (Section 2.4).

5.3.3. Predicted Change in *a* +4K Warmer Climate

Figure 7 shows a global increase of MTRH between 15°N and 15°S over the tropical oceans in the AMIP+4 K simulations with respect to the AMIP baseline simulation (+10%, Figure 7c), while almost no change in LTRH

(Figure 7e) apart from *a* +10% increase in Sc regions. These results yield a sharp decrease in RH_{DIFF} (Figure 7g) between 15°N and 15°S (−10%), while a sharp increase in Sc regions (+10%).

The model forced increase of tropical mean LTRH (+0.25%/K = +1%/4K, Figure 7e), MTRH (+1.5%/K = +6%/4K, Figure 7c), and UTRH (+1.25%/K = +5%/4K, Figure 7a) with warming are consistent in sign with their local scale increases in current climate model simulations (Figures 11d, 11e and 11f), as well as with the model tropical mean sensitivity to SST in the current climate (Figure 10).

Forced MTRH change (Figure 7c) occurs mostly over SSTs > 297 K (Figure 3), where the sensitivity of modeled MTRH to SST in current climate (+2.4%/K) is similar to—although 1.5 times larger than—the observations (Figure 11). Therefore, if the model reproduces the change between +4 K and current climate well, then the model prediction should be about right for MTRH. In contrast, the change in LTRH (Figure 7e) mostly occurs over SSTs < 297 K, where modeled LTRH (Figure 11d) in current climate increases strongly with SST in contrast to the observed decrease (Figure 11a). Therefore, the model prediction of LTRH to forced SST change might not be reliable, but this needs to be verified in future work with a dedicated set of RH model outputs with high vertical resolution in the boundary layer.

6. Discussion and Conclusions

6.1. Observations

We have analyzed how cloud properties and RH vary with SST in the presence of tropical low clouds (emission altitudes ≤3 km, no high clouds) in space-borne lidar and microwave radiometer observations. We performed our analyses on the local process scale on instantaneous and monthly mean timescales, where clouds and RH vary nonlinearly with SST, and compare them with the tropical mean scale, where clouds and RH vary quasi-linearly with SST on monthly and annual timescales. We split the tropical low clouds into two categories, opaque clouds ($\tau > 3$–5) and thin clouds ($\tau < 3$–5), which we show are coexisting in all regions of the tropics. We found different behaviors over SSTs < 297 K and SSTs > 297 K. Table S1 in the Supporting Information S1 summarizes the results in Figures 2–11.

Over SSTs < 297 K, the process scale observations show that the median C_{OPAQUE} decreases rapidly with SST (−6%/K), and typically faster in TrCu-Sc regions (about −6%/K) than in TrCu regions (about −1.5%/K). Simultaneously, the difference between lower- and middle-tropospheric RH (RH_{DIFF}), also decreases linearly with SST (−1.6%/K). Moreover, the opaque clouds shrink vertically as the median Z_{OpTOP} lowers (−100 m/K) and Z_{OpFA} stays constant. The simultaneous decreases of C_{OPAQUE} and RH_{DIFF} are consistent with the proposed literature mechanism that tropical low cloud cover decreases via more mixing between the moist boundary layer and dry free troposphere (Scott et al., 2020; Van der Dussen et al., 2015). However, Van der Dussen et al. (2015) found a thinning of the Sc layer when SST was perturbed by +2 K as Sc base height rose more than Sc top height in response to a greater dry air entrainment. In contrast, we observe vertically shrinking low opaque clouds due to linearly decreasing Z_{OpTOP} with SST. Regarding thin clouds, C_{THIN} is almost insensitive (+0.1%/K) to SST while Z_{THIN} rises linearly (+35 m/K) with SST. The vertical shrinkage of low opaque clouds and low thin cloud variations with SST in these regions are characterized here for the first time with satellite observations.

Over SSTs > 297 K, the median C_{OPAQUE} decreases weakly with SST (−1.5%/K) in the process scale observations, at about the same rate in both TrCu-Sc regions and TrCu regions. Simultaneously, RH_{DIFF} decreases nonlinearly/more rapidly (−3.6%/K) over SSTs > 297 K. Here, the vertical extent of low opaque clouds remains fairly constant, while the low opaque clouds descend with SST (about −55 m/K). The behavior of opaque clouds in these regions is consistent with Scott et al. (2020). Meanwhile, C_{THIN} decreases (−1.6%/K) while Z_{THIN} rises (+60 m/K). The rising Z_{THIN} is consistent with LES discussion about rising altitudes (Radtke et al., 2021; Rieck et al., 2012).

Overall, our observed covariations of opaque clouds and RH with SST suggest that as LTRH and RH_{DIFF} decrease with SST, wide and deep low opaque clouds over SSTs < 294 K transition into low opaque clouds of more shallow depth and smaller horizontal coverage over SSTs > 297 K.

When averaged over large areas, low cloud properties and RH vary roughly linearly with SST, as signatures identified on the process scale are typically smaller or no longer visible. The area-averaged behavior roughly corresponds to the process scale observations weighted by the SST distribution and is always dominated by one

population—not always the most numerous, sometimes the one most sensitive to SST change—and masks others. It is therefore difficult to compare previous works that reported linear covariations between low cloud sensitivity and SST to each other when they used different scales, subsamples, or areas. The results of our study bridge such gaps as it lays out instantaneous variations of low clouds and RH to SST and links them with the annual tropical mean scale. For example, our analysis of observations on different time and space scales shows that annual/monthly tropical mean variations of C_{OPAQUE} and LTRH with SST seem to carry signatures of process scale variations over SSTs > 297 K, while annual/monthly tropical mean variations of C_{THIN} and MTRH seem to exhibit behaviors of process scale variations over SSTs < 297 K.

Our results are presented for daytime data only (01:30p.m.), while clouds and RH have diurnal variations. Therefore, we also analyzed nighttime observations around 01:30a.m. (not shown) of these tropical low clouds to verify the robustness of our results. We found variations with SST similar to daytime, but during night, tropical low cloud altitudes are a little lower, and C_{OPAQUE} is greater, while C_{THIN} is smaller, consistent with previous work (e.g., Chepfer et al., 2019; Noel et al., 2018).

6.2. Model Evaluation

We repeated the same analyses as we performed for the observations with simulations from the IPSL-CM6A climate model with the COSP/lidar simulator to ensure apple-to-apple cloud comparison between observations and model.

Like the observations, the model also simulates different sensitivities of low clouds to SST over cold (SSTs < 297.5 K) and warm SSTs (SSTs > 299 K), but the transition between those regions is clearly too rapid in the model compared to the observations, as C_{OPAQUE} drops from 100% to 10% over only a 1.5 K SST range in the model (297.5–299 K). Over SSTs < 297.5 K, the model correctly simulates decreasing monthly C_{OPAQUE}, rising Z_{THIN}, and increasing MTRH with increasing SST but fails to reproduce variations of Z_{OPAQUE}, Z_{OpTOP}, C_{THIN}, and LTRH. Regarding LTRH, we cannot be entirely sure that the differences between model and observations are real. But as a result, contrary to the observations, the model produces increasing $\mathrm{RH}_{\mathrm{DIFF}}$ and no vertical shrinkage of opaque clouds.

When looking at the tropical mean scale, the model reproduces the observed increases of monthly MTRH and UTRH and the sign of the cloud sensitivities to SST, but not the magnitudes. For example, the sensitivity of monthly C_{OPAQUE} to SST is overestimated in the model (−16.8%/K instead of −4.5%/K) possibly due to the too strong transition highlighted above.

Model simulations show that as climate warms (+4 K), clouds change the most over SSTs 297.5–299 K. Assuming that the model captures the evolution of the sensitivity from current to warmer climate, and assuming that the variable is well reproduced by the model in the current climate, we find that the predicted increase in tropical mean MTRH as climate warms is plausible, the predicted decrease in regional C_{OPAQUE} is correct but its magnitude is likely overestimated, and the predicted regional changes in low opaque cloud altitudes, and thin cloud properties are likely less reliable.

Data Availability Statement

GOCCP data is available through CFMIP-OBS (https://climserv.ipsl.polytechnique.fr/cfmip-obs/), and SAPHIR data through the Aeris/ICARE ground segment of Megha-Tropiques (https://www.icare.univ-lille.fr/product-documentation/?product=SAPHIR-L2B-RH).

Acknowledgments
We thank NASA and CNES for data accessibility, and CNES for financial support through the EECLAT and Megha-Tropiques projects. We thank the national Aeris data center that hosts the satellite data, and the computing resources of ESPRI/IPSL were greatly appreciated. We thank Patrick Raberanto (LMD/IPSL), Christophe Dufour (LATMOS/IPSL), and Artem Feofilov (LMD/IPSL), respectively, for the gridded GOCCP, SAPHIR L2B, and model data sets. We thank the two anonymous reviewers who helped us to significantly improve the manuscript.

References

Ackerley, D., Chadwick, R., Dommenget, D., & Petrelli, P. (2018). An ensemble of AMIP simulations with prescribed land surface temperatures. *Geoscientific Model Development*, *11*, 3865–3881. https://doi.org/10.5194/gmd-11-3865-2018

Andrews, T., & Webb, M. (2018). The dependence of global cloud and lapse rate feedbacks on the spatial structure of tropical Pacific warming. *Journal of Climate*, *31*, 641–654. https://doi.org/10.1175/JCLI-D-17-0087.1

Bates, J. J., & Jackson, D. L. (2001). Trends in upper-tropospheric humidity. *Geophysical Research Letters*, *28*, 1695–1698. https://doi.org/10.1029/2000gl012544

Behrangi, A., Kubar, T., & Lambrigtsen, B. (2012). Phenomenological description of tropical clouds using CloudSat cloud classification. *Monthly Weather Review*, *140*, 3235–3249. https://doi.org/10.1175/mwr-d-11-00247.1

Bodas-Salcedo, A., Webb, M. J., Bony, S., Chepfer, H., Dufresne, J.-L., Klein, S. A., et al. (2011). COSP: Satellite simulation software for model assessment. *Bulletin of the American Meteorological Society*, *92*, 1023–1043. https://doi.org/10.1175/2011bams2856.1

Boggs, P. T., Byrd, R. H., Rogers, J. E., & Schnabel, R. B. (1992). User's Reference Guide For ODRPACK Version 2.01 Software for Weighted Orthogonal Distance Regression. NISTIR 4834. *Applied and Computational Mathematics Division*, Computing and Applied Mathematics Laboratory, U.S. DEPARTMENT OF COMMERCE, National Institute of Standards and Technology.

Boggs, P. T., & Rogers, J. E. (1990). Orthogonal distance Regression. NISTIR 89-4197. *Applied and computational mathematics division*, Center for Computing and Applied Mathematics. U.S. DEPARTMENT OF COMMERCE, National Institute of Standards and Technology.

Boggs, P. T., Spiegelman, C. H., Donaldson, J. R., & Schnabel, R. B. (1988). A computational examination of orthogonal distance regression. *Journal of Econometrics*, *38*, 169–201. https://doi.org/10.1016/0304-4076(88)90032-2

Bony, S., & Dufresne, J.-L. (2005). Marine boundary layer clouds at the heart of tropical cloud feedback uncertainties in climate models. *Geophysical Research Letters*, *32*. https://doi.org/10.1029/2005GL023851

Bony, S., Stevens, B., Frierson, D. M. W., Jakob, C., Kageyama, M., Pincus, R., et al. (2015). Clouds, circulation and climate sensitivity. *Nature Geoscience*, *8*, 261–268. https://doi.org/10.1038/NGEO2398

Bretherton, C. S., Blossey, P. N., & Jones, C. R. (2013). Mechanisms of marine low cloud sensitivity to idealized climate perturbations: A single-LES exploration extending the CGILS cases. *Journal of Advances in Modeling Earth Systems*, *5*, 316–337. https://doi.org/10.1002/jame.20019

Brient, F., & Bony, S. (2013). Interpretation of the positive low-cloud feedback predicted by a climate model under global warming. *Climate Dynamics*, *40*, 2415–2431. https://doi.org/10.1007/s00382-011-1279-7

Brient, F., Schneider, T., Tan, Z., Bony, S., Qu, X., & Hall, A. (2016). Shallowness of tropical low clouds as a predictor pf climate models' response to warming. *Climate Dynamics*, *47*, 433–449. https://doi.org/10.1007/s00382-015-2846-0

Brogniez, H., Fallourd, R., Mallet, C., Sivira, R., & Dufour, C. (2016). Estimating confidence intervals around relative humidity profiles from satellite observations: Applications to the SAPHIR sounder. *Journal of Atmospheric and Oceanic Technology*, *33*, 1005–1022. https://doi.org/10.1175/jtech-d-15-0237.1

Brogniez, H., Kirstetter, P.-E., & Eymard, L. (2013). Expected improvements in the atmospheric humidity profile retrieval using the Megha-Tropiques microwave payload. *Quarterly Journal of the Royal Meteorological Society*, *139*, 842–851. https://doi.org/10.1002/qj.1869

Caldwell, P. M., Zelinka, M. D., Taylor, K. E., & Marvel, K. (2016). Quantifying the sources of intermodel spread in equilibrium climate sensitivity. *Journal of Climate*, *29*, 513–524. https://doi.org/10.1175/JCLI-D-15-0352.1

Ceppi, P., Brient, F., Zelinka, M. D., & Hartmann, D. L. (2017). Cloud feedback mechanisms and their representation in global climate models. *WIREs Clim Change*, *2017*, e465. https://doi.org/10.1002/wcc.465

Cesana, G., Del Genio, A. D., Ackerman, A. S., Kelley, M., Elsaesser, G., Fridlind, A. M., et al. (2019). Evaluating models' response of tropical low clouds to SST forcings using CALIPSO observations. *Atmospheric Chemistry and Physics*, *19*, 2813–2832. https://doi.org/10.5194/acp-19-2813-2019

Cesana, G., Del Genio, A. D., & Chepfer, H. (2019). The cumulus and stratocumulus CloudSat-CALIPSO Dataset (CASCCAD). *Earth System Science Data*, *11*, 1745–1764. https://doi.org/10.5194/essd-11-1745-2019

Cesana, G. V., & Del Genio, A. D. (2021). Observational constraint on cloud feedbacks suggests moderate climate sensitivity. *Nature Climate Change*, *11*, 213–218. https://doi.org/10.1038/s41558-020-00970-y

Chepfer, H., Bony, S., Winker, D., Cesana, G., Dufresne, J. L., Minnis, P., et al. (2010). The GCM-oriented CALIPSO cloud product (CALIPSO-GOCCP). *Journal of Geophysical Research*, *115*, 1–13. https://doi.org/10.1029/2009jd012251

Chepfer, H., Bony, S., Winker, D., Chiriaco, M., Dufresne, J.-L., & Sèze, G. (2008). Use of CALIPSO lidar observations to evaluate the cloudiness simulated by a climate model. *Geophysical Research Letters*, *35*. https://doi.org/10.1029/2008GL034207

Chepfer, H., Brogniez, H., & Noel, V. (2019). Diurnal variations of cloud and relative humidity profles across the tropics. *Nature Scientific Reports*, *9*. https://doi.org/10.1038/s41598-019-52437-6

Chung, D., & Teixeira, J. (2012). A simple model for stratocumulus to shallow cumulus transitions. *Journal of Climate*, *25*, 2547–2554. https://doi.org/10.1175/JCLI-D-11-00105.1

Colman, R. A., & Hanson, L. I. (2013). On atmospheric radiative feedbacks associated with climate variability and change. *Climate Dynamics*, *40*, 475–492. https://doi.org/10.1007/s00382-012-1391-3

De Szoke, S. P., Verlinden, K. L., Yuter, S. E., & Mechem, D. B. (2016). The time scales of variability of marine low clouds. *Journal of Climate*, *29*, 6463–6481. https://doi.org/10.1175/JCLI-D-15-0460.1

Dee, D. P., Uppala, S. M., Simmons, A. J., Berrisford, P., Poli, P., Kobayashi, S., et al. (2011). The ERA-interim reanalysis: Configuration and performance of the data assimilation system. *Quarterly Journal of the Royal Meteorological Society*, *137*, 553–597. https://doi.org/10.1002/qj.828

Eastman, R., Warren, S. G., & Hahn, C. J. (2011). Variations in cloud cover and cloud types over the ocean from surface observations, 1945-2008. *Journal of Climate*, *24*, 5914–5934. https://doi.org/10.1175/2011jcli3972.1

Eymard, L., Gheudin, M., Laborie, P., Sirou, F., Le Gac, C., Vinson, J. P., et al. (2002). The SAPHIR humidity sounder. *Notes Act. Instrum. de l'IPSL*, *24*.

Fasullo, J. T., & Trenberth, K. E. (2012). A less cloudy future: The role of subtropical subsidence in climate sensitivity. *Science*, *338*, 792–794. https://doi.org/10.1126/science.1227465

Fisher, R. A. (1956). *Statistical methods and scientific inference*. Hafner.

Forster, P. M., Richardson, T., Maycock, A. C., Smith, C. J., Samset, B. H., Myhre, G., et al. (2016). Recommendations for diagnosing effective radiative forcing from climate models for CMIP6. *Journal of Geophysical Research: Atmospheres*, *121*, 12460–12475. https://doi.org/10.1002/2016JD025320

Fueglistaler, S. (2019). Observational evidence for two modes of coupling between sea surface temperatures, tropospheric temperature profile, and shortwave cloud radiative effect in the tropics. *Geophysical Research Letters*, *46*, 9890–9898. https://doi.org/10.1029/2019GL083990

Guzman, R., Chepfer, H., Noel, V., Vaillant de Guélis, T., Kay, J. E., Raberanto, P., et al. (2017). Direct atmosphere opacity observations from CALIPSO provide new constraints on cloud-radiation interactions. *Journal of Geophysical Research: Atmospheres*, *122*, 1066–1085. https://doi.org/10.1002/2016jd025946

Hoffmann, L., Günther, G., Li, D., Stein, O., Wu, X., Griessbach, S., et al. (2018). From ERA-interim to ERA5: Considerable impact of ECMWF's next-generation reanalysis on Lagrangian transport simulations. *Atmospheric Chemistry and Physics*, 1–38. https://doi.org/10.5194/acp-2018-1199

Höjgård-Olsen, E., Brogniez, H., & Chepfer, H. (2020). Observed evolution of the tropical atmospheric water cycle with sea surface temperature. *Journal of Climate*, *33*, 3449–3470. https://doi.org/10.1175/JCLI-D-19-0468.1

Hourdin, F., Jam, A., Rio, C., Couvreux, F., Sandu, I., Lefebvre, M.-P., et al. (2019). Unified parameterization of convective boundary layer transport and clouds with the thermal plume model. *Journal of Advances in Modeling Earth Systems*, *11*. https://doi.org/10.1029/2019MS001666

Hourdin, F., Musat, I., Bony, S., Braconnot, P., Codron, F., Dufresne, J.-L., et al. (2006). The LMDZ4 general circulation model: Climate performance and sensitivity to parametrized physics with emphasis on tropical convection. *Climate Dynamics*, *27*, 787–813. https://doi.org/10.1007/s00382-006-0158-0

Hourdin, F., Rio, C., Grandpeix, J.-Y., Madeleine, J.-B., Cheruy, F., Rochetin, N., et al. (2020). LMDZ6A: The atmospheric component of the IPSL climate model with improved and better tuned physics. *Journal of Advances in Modeling Earth Systems*, *12*, e2019MS001892. https://doi.org/10.1029/2019ms001892

Hourdin, F., Rio, C., Jam, A., Traore, A.-K., & Musat, I. (2020). Convective boundary layer control of the sea surface temperature in the tropics. *Journal of Advances in Modeling Earth Systems*, *12*, e2019MS001988. https://doi.org/10.1029/2019MS001988

Kamae, Y., Ogura, T., Shiogama, H., & Watanabe, H. (2016). Recent progress toward reducing the uncertainty in tropical low cloud feedback and climate sensitivity: Review. *Geoscience Letters*, *3*. https://doi.org/10.1186/s40562-016-0053-4

Klein, S. A., & Hall, A. (2015). Emergent constraints for cloud feedbacks. *Current Climate Change Reports*, *1*, 276–287. https://doi.org/10.1007/s40641-015-0027-1

Klein, S. A., Hall, A., Norris, J. R., & Pincus, R. (2017). Low-cloud feedbacks from cloud controlling factors: A review. *Surveys in Geophysics*, *38*, 1307–1329. https://doi.org/10.1007/s10712-017-9433-3

Leng, L., Zhang, T., Kleinman, L., & Zhu, W. (2007). Ordinary least square regression, orthogonal distance regression, geometric mean regression and their applications in aerosol science. *Journal of Physics: Conference Series, IOP Publishing*. *78*. https://doi.org/10.1088/1742-6596/78/1/012084

Loeb, N. G., Wang, H., Allan, R., Andrews, T., Armour, K., Cole, J. N. S., et al. (2020). New generation of climate models track recent unprecedented changes in Earth's radiation budget observed by CERES. *Geophysical Research Letters*, *47*, e2019GL086705. https://doi.org/10.1029/2019gl086705

Lolli, B., & Gasperini, P. (2012). A comparison among general orthogonal regression methods applied to earthquake magnitude conversions. *Geophysical Journal International*, *190*, 1135–1151. https://doi.org/10.1111/j.1365-246X.2012.05530.x

Madeleine, J.-B., Hourdin, F., Grandpeix, J.-Y., Rio, C., Dufresne, J.-L., Vignon, E., et al. (2020). Improved representation of clouds in the atmospheric component LMDZ6A of the IPSL-CM6A earth system model. *Journal of Advances in Modeling Earth Systems*, *12*, e2020MS002046. https://doi.org/10.1029/2020MS002046

Mauritsen, T., Graversen, R. G., Klocke, D., Langen, P. L., Stevens, B., & Tomassini, L. (2013). Climate feedback efficiency and synergy. *Climate Dynamics*, *41*, 2539–2554. https://doi.org/10.1007/s00382-013-1808-7

McCoy, D. T., Eastman, R., Hartmann, D. L., & Wood, R. (2017). The change in low cloud cover in a warmed climate inferred from AIRS, MODIS, and ERA-interim. *Journal of Climate*, *30*, 3609–3620. https://doi.org/10.1175/JCLI-D-15-0734.1

Myers, T. A., & Norris, J. R. (2013). Observational evidence that enhanced subsidence reduces subtropical marine boundary layer cloudiness. *Journal of Climate*, *26*. https://doi.org/10.1175/JCLI-D-12-00736.1

Myers, T. A., & Norris, J. R. (2015). On the relationships between subtropical clouds and meteorology in observations and CMIP3 and CMIP5 models. *Journal of Climate*, *28*. https://doi.org/10.1175/JCLI-D-14-00475.1

Myers, T. A., & Norris, J. R. (2016). Reducing the uncertainty in subtropical cloud feedback. *Geophysical Research Letters*, *43*, 2144–2148. https://doi.org/10.1002/2015GL067416

Noel, V., Chepfer, C., Chiriaco, M., & Yorks, J. (2018). The diurnal cycle of cloud profiles over land and ocean between 51°S and 51°N, seen by the CATS spaceborne lidar from the International Space Station. *Atmospheric Chemistry and Physics*, *18*, 9457–9473. https://doi.org/10.5194/acp-18-9457-2018

Nuijens, L., & Siebesma, A. P. (2019). Boundary layer clouds and convection over subtropical oceans in our current and in a warmer climate. *Current Climate hange Reports*, *5*, 80–94. https://doi.org/10.1007/s40641-019-00126-x

Orlanski, I. (1975). A rational subdivision of scales for atmospheric processes. *Bulletin of the American Meteorological Society*, *56*, 527–530.

Perpina, M., Noel, V., Chepfer, H., Guzman, R., & Feofilov, A. (2021). Link between opaque cloud properties and atmospheric dynamics in observations and simulations of current climate in the tropics, and impact on future predictions. *Journal of Geophysical Research: Atmospheres*, *126*. https://doi.org/10.1029/2020jd033899

Qu, X., Hall, A., Klein, S. A., & Caldwell, P. M. (2014). On the spread of changes in marine low cloud cover in climate model simulations of the 21st century. *Climate Dynamics*, *42*, 2603–2626. https://doi.org/10.1007/s00382-013-1945-z

Qu, X., Hall, A., Klein, S. A., & DeAngelis, A. M. (2015). Positive tropical marine low-cloud cover feedback inferred from cloud-controlling factors. *Geophysical Research Letters*, 7767–7775. https://doi.org/10.1002/2015GL065627

Radtke, J., Mauritsen, T., & Hohenegger, C. (2021). Shallow cumulus cloud feedback in large eddy simulations – Bridging the gap to storm-resolving models. *Atmospheric Chemistry and Physics*, *21*, 3275–3288. https://doi.org/10.5194/acp-21-3275-2021

Rieck, M., Nuijens, L., & Stevens, B. (2012). Marine boundary layer cloud feedbacks in a constant relative humidity atmosphere. *Journal of the Atmospheric Sciences*, *69*. https://doi.org/10.1175/JAS-D-11-0203.1

Roca, R., Brogniez, H., Chambon, P., Chomette, O., Cloché, S., Gosset, M. E., et al. (2015). The megha-tropiques mission: A review after three years in orbit. *Frontiers of Earth Science*, *3*, 1–14. https://doi.org/10.3389/feart.2015.00017

Scott, R. C., Myers, T. A., Norris, J. R., Zelinka, M. D., Klein, S. A., Sun, M., & Doelling, D. R. (2020). Observed sensitivity of low-cloud radiative effects to meteorological perturbations over the global oceans. *Journal of Climate*, *33*, 7717–7734. https://doi.org/10.1175/JCLI-D-19-1028.1

Sherwood, S. C., Ingram, W., Tsushima, Y., Satoh, M., Roberts, M., Vidale, P. L., & O'Gorman, P. A. (2010). Relative humidity changes in a warmer climate. *Journal of Geophysical Research*, *115*. https://doi.org/10.1029/2009JD012585

Sherwood, S. C., Webb, M. J., Annan, J. D., Armour, K. C., Forster, P. M., Hargreaves, J. C., et al. (2020). An assessment of Earth's climate sensitivity using multiple lines of evidence. *Reviews of Geophysics*, *58*, e2019RG000678. https://doi.org/10.1029/2019rg000678

Shi, L., & Bates, J. J. (2011). Three decades of intersatellite-calibrated High-Resolution Infrared Radiation Sounder upper tropospheric water vapor. *Journal of Geophysical Research*, *116*. https://doi.org/10.1029/2010JD014847

Sivira, R. G., Brogniez, H., Mallet, C., & Oussar, Y. (2015). A layer-average relative humidity profile retrieval for microwave observations: Design and results for the megha-tropiques payload. *Atmospheric Measurement Techniques*, *8*, 1055–1071. https://doi.org/10.5194/amt-8-1055-2015

Steyn, D. G., Oke, T. R., Hay, J. E., & Knox, J. L. (1981). *On the scales in meteorology and climate*.

Swales, D. J., Pincus, R., & Bodas-Salcedo, A. (2018). The cloud feedback model Intercomparison Project observational simulator package: Version 2 (COSP2), geophys. *Mod. Dev.*, *11*(1), 77–81. https://doi.org/10.5194/gmd-11-77-2018

Vaillant de Guélis, T., Chepfer, H., Guzman, R., Bonazzola, M., Winker, D. M., & Noel, V. (2018). Space lidar observations constrain longwave cloud feedback. *Nature Scientific Reports*, *8*. https://doi.org/10.1038/s41598-018-34943-1

Vaillant de Guélis, T., Chepfer, H., Noel, V., Guzman, R., Dubuisson, P., Winker, D. M., & Kato, S. (2017). The link between outgoing longwave radiation and the altitude at which a spaceborne lidar beam is fully attenuated. *Atmospheric Measurement Techniques*, *10*, 4659–4685.

Van der Dussen, J. J., de Roode, S. R., Dal Gesso, S., & Siebesma, A. P. (2015). An LES model study of the influence of the free tropospheric thermodynamic conditions on the stratocumulus response to a climate perturbation. *Journal of Advances in Modeling Earth Systems*, *7*, 670–691. https://doi.org/10.1002/2014MS000380

Vial, J., Bony, S., Stevens, B., & Vogel, R. (2017). Mechanisms and model diversity of trade-wind shallow cumulus cloud feedbacks: A review. *Surveys in Geophysics*, *38*, 1331–1353. https://doi.org/10.1007/s10712-017-9418-2

Vial, J., Dufresne, J.-L., & Bony, S. (2013). On the interpretation of inter-model spread in CMIP5 climate sensitivity estimates. *Climate Dynamics*, *41*, 3339–3362. https://doi.org/10.1007/s00382-013-1725-9

Winker, D. M., Vaughan, M. A., Omar, A., Hu, Y., & Powell, K. A. (2009). Overview of the CALIPSO mission and CALIOP data processing algorithms. *Journal of Atmospheric and Oceanic Technology*, *26*, 2310–2323. https://doi.org/10.1175/2009jtecha1281.1

Wyant, M. C., Bretherton, C. S., Rand, H. A., & Stevens, D. E. (1997). Numerical simulations and a conceptual model of the stratocumulus to trade cumulus transition. *Journal of the Atmospheric Sciences*, *54*, 168–192. https://doi.org/10.1175/1520-0469(1997)054<0168:nsaacm>2.0.co;2

Zelinka, M. D., Klein, S. A., & Hartmann, D. L. (2012). Computing and Partitioning cloud feedbacks using cloud property histograms. Part II: Attribution to changes in cloud amount, altitude, and optical depth. *Journal of Climate*, *25*, 3736–3754. https://doi.org/10.1175/JCLI-D-11-00249.1

Zelinka, M. D., Klein, S. A., Taylor, K. E., Andrews, T., Webb, M., Gregory, J. M., & Forster, P. M. (2013). Contributions of different cloud types to feedbacks and rapid adjustments in CMIP5. *Journal of Climate*, 5007–5027. https://doi.org/10.1175/JCLI-D-12-00555.1

Zelinka, M. D., Myers, T. A., McCoy, D. T., Po-Chedley, S., Caldwell, P. M., Ceppi, P., et al. (2020). Causes of higher climate sensitivity in CMIP6 models. *Geophysical Research Letters*, *47*, e2019GL085782. https://doi.org/10.1029/2019GL085782

Zelinka, M. D., Zhou, C., & Klein, S. A. (2016). Insights from a refined decomposition of cloud feedbacks. *Geophysical Research Letters*, *43*, 9259–9269. https://doi.org/10.1002/2016GL069917

Zhai, C., Jiang, J. H., & Su, H. (2015). Long-term cloud change imprinted in seasonal cloud variation: More evidence of high climate sensitivity. *Geophysical Research Letters*, *42*, 8729–8737. https://doi.org/10.1002/2015GL065911

Zhou, C., Zelinka, M. D., Dessler, A. E., & Klein, S. A. (2015). The relationship between interannual and long-term cloud feedbacks. *Geophysical Research Letters*, *42*(463–10), 10469. https://doi.org/10.1002/2015GL066698

Zhou, C., Zelinka, M. D., Dessler, A. E., & Yang, P. (2013). An analysis of the short-term cloud feedback using MODIS data. *Journal of Climate*, *26*, 4803–4815. https://doi.org/10.1175/JCLI-D-12-00547.1

Zhou, C., Zelinka, M. D., & Klein, S. A. (2016). Impact of decadal cloud variations on the Earth's energy budget. *Nature Geoscience*. https://doi.org/10.1038/NGEO2828

Zhou, C., Zelinka, M. D., & Klein, S. A. (2017). Analyzing the dependence of global cloud feedback on the spatial pattern of sea surface temperature change with a Green's function approach. *Journal of Advances in Modeling Earth Systems*, *9*, 2174–2189. https://doi.org/10.1002/2017MS001096

Reference From the Supporting Information

Noel, V., Chepfer, H., Hoareau, C., Reverdy, M., & Cesana, G. (2014). Effect of solar activity and geomagnetic field on noise in CALIOP profiles ABOVE South Atlantic Anomaly. *Atmospheric Measurement Techniques*. https://doi.org/10.5194/amt-7-1597-2014